

Banner appropriate to article type will appear here in typeset article

Log–linear law of the mean streamwise velocity in turbulent boundary layers with moderate adverse pressure gradients

Fuzhou Lyu¹, Lihao Zhao¹, Weixi Huang¹, and Chunxiao Xu¹

¹ AML, Department of Engineering Mechanics, Tsinghua University, Beijing 100084, People's Republic of China

Corresponding author: Chunxiao Xu, xucx@tsinghua.edu.cn

(Received xx; revised xx; accepted xx)

An essential feature of canonical zero-pressure-gradient (ZPG) turbulent boundary layers (TBLs) is that the mean streamwise velocity exhibits a logarithmic dependence on the wall-normal distance, known as the log law. In this study, we demonstrate that this conventional log law is not suitable for turbulent boundary layers subjected to pressure gradients (PGs). Instead, a log–linear law is theoretically derived for TBLs under moderate adverse pressure gradients (APGs), based on the total shear-stress balance and a rescaled eddy-viscosity model. The validity of the proposed log–linear law is assessed using available datasets of incompressible APG TBLs with the Clauser pressure-gradient parameter β ranging from 0.73 to 9.0. Compared with the conventional log law, the present log–linear formulation shows significantly improved agreement with the measured mean velocity profiles. In the limiting case of $\beta \rightarrow 0$, the proposed law naturally recovers the classical log law.

1. Introduction

TBLs are classical flow configurations that have been extensively studied for decades due to their practical applications and theoretical importance. Most of the previous studies of TBL focus on the canonical ZPG cases. On the other hand, compared with ZPG TBLs, TBLs with pressure gradients are more common in practical applications such as aircraft wings and turbine blades. Due to the advances of experimental and numerical techniques, studies of PG TBLs have become increasingly active in the past decade. However, some fundamental issues remain unresolved, especially regarding the applicability of the conventional log law to PG TBLs.

For canonical ZPG TBLs, the log law states that the mean streamwise velocity U in the overlap region between the inner and outer layers follows a logarithmic dependence on the wall-normal distance y , i.e.,

$$U_{log}^+ = \frac{1}{\kappa} \ln y^+ + B, \quad (1.1)$$

where the superscript + denotes normalization by wall units, defined using the friction velocity u_τ and the viscous length scale δ_ν , with $u_\tau = \sqrt{\tau_w/\rho}$ and $\delta_\nu = \nu/u_\tau$. Here, τ_w is the wall shear stress, and ρ and ν are the fluid density and kinematic viscosity, respectively. The Kármán constant is typically taken as $\kappa \approx 0.41$, while $B \approx 5.0$ denotes the intercept of the log law. This simple equation laid the foundation for understanding wall-bounded turbulent flows (Pope 2000; White & Majdalani 2006), and has been widely employed in Reynolds-averaged Navier-Stokes (RANS) models (Wilcox *et al.* 1998) and wall-modeled large eddy simulation (WMLES) (Larsson *et al.* 2016). The region where the log law holds is usually referred to as the log region. Here, we use the term “intermediate region” to refer to the conventional log region, as we will show later that the log law is not applicable to APG TBLs.

When pressure gradients are included, the flow properties become more complex. In particular, it has been recognized that the mean velocity profiles in the intermediate region of APG TBLs shift below the log law of ZPG TBLs (Nagano *et al.* 1998; Devenport & Lowe 2022) and the slope of the log law changes with the pressure gradient (Skaare & Krogstad 1994). Traditionally, these deviations are attributed to the variation of the Kármán constant κ . For instance, Nickels (2004), Nagib & Chauhan (2008), Chauhan *et al.* (2010), and Monty *et al.* (2011) all reported lower values of κ for APG TBLs compared to the standard value of 0.41 for ZPG TBLs. In addition, studies by Huang & Bradshaw (1995), Monty *et al.* (2011) and Lee (2017) show that the wall-normal range where the log law holds is also reduced for APG TBLs, even when the Kármán constant has been modified. These issues pose challenges to the analysis and modeling of APG TBLs. For example, Crook (2002) summarized that a ± 0.5 change in $1/\kappa$ results in a 12% difference in u_τ , which corresponds to an uncertainty of approximately 25% in the friction coefficient. Furthermore, the reduction of the effective range of the log law makes WMLES sensitive to the choice of the matching layer, as this layer is usually required to be placed in the log region (Baggett 1997). Therefore, it is necessary to reevaluate the applicability of the log law in APG TBLs and develop a more general velocity law that can better capture the behavior of APG TBLs.

The objective of the present study is to develop such a velocity law that is more robust than the conventional log law and explicitly accounts for pressure gradient effects. As will be shown later, both the apparent variation of the Kármán constant κ and the reduction in the effective range of the log law can be attributed to the inapplicability of the classical log law to APG turbulent boundary layers. To address this limitation, a new log–linear law is proposed. Compared with the conventional log law, the proposed formulation exhibits a substantially wider range of validity, while the Kármán constant κ retains its classical value of 0.41. Within this framework, the classical log law emerges as a special case of the log–linear law in the absence of a pressure gradient.

2. log–linear law for APG TBLs

For canonical ZPG TBLs, the log law can be derived from the eddy viscosity hypothesis and the total-shear-stress equation, leading to

$$\frac{\nu_t}{\nu} \frac{\partial U^+}{\partial y^+} = \tau_t^+, \quad (2.1)$$

where ν_t is the eddy viscosity. In the intermediate layer, it is commonly assumed that

$$\nu_t/\nu = \kappa y^+. \quad (2.2)$$

In Eq. (2.1), the left-hand side represents the Reynolds shear stress under the eddy viscosity assumption, while the viscous stress is neglected. The right-hand side is the total shear stress τ_t^+ . In the near-wall region of ZPG TBLs, $\tau_t^+ \approx 1$ is a good approximation. Therefore, substituting $\tau_t^+ \approx 1$ and $\nu_t/\nu = \kappa y^+$ into Eq. (2.1) and then integrating with respect to y^+ yields the log law. Equation (2.1) is derived from the momentum equation and is thus applicable to APG TBLs. However, the other two assumptions, namely $\tau_t^+ \approx 1$ and $\nu_t/\nu = \kappa y^+$, need to be revisited in the context of pressure gradients.

To quantitatively assess the strength of the pressure gradient, the Clauser pressure gradient parameter $\beta = (\delta_d/\tau_w)(dP_e/dx)$ is considered, where δ_d is the displacement thickness, x is the streamwise coordinate, and P_e is the pressure at the edge of the boundary layer (Clauser 1954). This parameter has been extensively used in studies of APG TBLs (Bobke *et al.* 2017; Devenport & Lowe 2022; Wei & Knopp 2023). Systematic comparisons by Monty *et al.* (2011) also show that β consistently collapses APG flow statistics and thus serves as an effective descriptor of PG effects.

We first reconsider the assumption $\tau_t^+ \approx 1$. The Reynolds-averaged momentum equation for turbulent boundary layers with pressure gradients reads

$$U \frac{\partial U}{\partial x} + V \frac{\partial U}{\partial y} = -\frac{1}{\rho} \frac{dP_e}{dx} - \frac{\partial \overline{u'v'}}{\partial y} + \nu \frac{\partial^2 U}{\partial y^2}, \quad (2.3)$$

where V is the mean wall-normal velocity and $\overline{u'v'}$ is the Reynolds shear stress. In the case of strong pressure gradients where the flow tends to separate, the Reynolds normal stresses neglected in Eq. (2.3) become significant (Simpson *et al.* 1977), and thus the present analysis is limited to moderate APGs. Integrating Eq. (2.3) in the near-wall region and neglecting the convective terms yields the following total shear stress relation:

$$\frac{\tau_t}{\rho} = \nu \frac{\partial U}{\partial y} - \overline{u'v'} \approx \left(1 + \beta \frac{y}{\delta_d}\right) \frac{\tau_w}{\rho}. \quad (2.4)$$

Thus, τ_t^+ is no longer constant in the near-wall region, but instead varies linearly with the wall-normal distance due to PG effects.

In the presence of pressure gradients, the assumption $\nu_t/\nu = \kappa y^+$ may no longer hold either. The wall coordinate y^+ is defined as the wall distance normalized by the viscous length scale δ_ν . Since δ_ν depends entirely on the wall shear stress τ_w , the normalization based on δ_ν is appropriate for ZPG TBLs, where the total shear stress τ_t is approximately constant in the near-wall region. However, for TBLs with pressure gradients, the distribution of τ_t is strongly influenced by PG effects, as observed by Perry *et al.* (1994). Therefore, there is no compelling reason to retain the assumption $\nu_t/\nu = \kappa y/\delta_\nu$. An alternative approach is to consider the Kármán momentum integral equation. For PG TBLs, this equation can be written as

$$\frac{d}{dx}(U_e^2 \theta) = u_\tau^2 (1 + \beta), \quad (2.5)$$

where θ is the momentum thickness and the subscript e denotes quantities at the edge of the boundary layer. According to Eq. (2.5), a new velocity scale and the corresponding length scale can be defined as

$$\begin{aligned} u_\beta &= u_\tau \sqrt{1 + \beta}, \\ \delta_\beta &= \frac{\nu}{u_\beta}. \end{aligned} \quad (2.6)$$

With these definitions, Eq. (2.5) can be rewritten as $d(U_e^2 \theta)/dx = u_\beta^2$, which has the same form as that for ZPG TBLs. This set of scales has been employed to model the mean

profiles of APG TBLs by Shu & Xu (2025). Replacing δ_v in Eq. (2.2) with δ_β yields

$$\frac{\nu_t}{\nu} = \kappa y^+ \sqrt{1 + \beta}. \quad (2.7)$$

Substituting Eqs. (2.7) and (2.4) into Eq. (2.1) gives

$$\kappa y^+ \sqrt{1 + \beta} \frac{\partial U^+}{\partial y^+} = 1 + \beta \frac{y}{\delta_d}. \quad (2.8)$$

Integrating Eq. (2.8) with respect to y^+ yields the refined law for the mean streamwise velocity:

$$U^+ = \frac{1}{\sqrt{1 + \beta}} \frac{1}{\kappa} \ln y^+ + \frac{\beta}{\sqrt{1 + \beta}} \frac{y^+}{\kappa \delta_d^+} + C, \quad (2.9)$$

where C is an integration constant. In contrast to Eq. (1.1), Eq. (2.9) contains a linear contribution in addition to the logarithmic term, and is therefore referred to as the log-linear law. Furthermore, when $\beta = 0$, Eq. (2.9) reduces to the log law in Eq. (1.1). Thus, the present log-linear law can be viewed as a generalization of the conventional log law for APG TBLs.

3. Validation of the proposed law

To assess the validity of the proposed log-linear law, APG TBL cases from four research groups are considered, as summarized in table 1. All datasets are obtained from direct numerical simulation (DNS) or high-fidelity large-eddy simulation (LES). The cases are named according to the following convention: the prefix ‘B’ denotes cases with a nearly constant Clauser parameter, where the subsequent number indicates the approximate value of β . For cases where β varies significantly along the streamwise direction, the prefix ‘M’ is used, followed by a number representing the exponent of the power-law free-stream velocity distribution $U_\infty \propto (x - x_0)^m$ applied at the upper boundary. This identifier is followed by the first letter of the first author’s surname and the year of publication. For instance, B10B2017 corresponds to the case with $\beta \approx 1.0$ from Bobke *et al.* (2017). For cases B10B2017–B14P2022, data are available at multiple streamwise stations, and the ranges of momentum thickness Reynolds number Re_θ , friction Reynolds number Re_τ , and Clauser parameter β are provided. For B07L2017–B90L2017, only one flow section is available for each case, and the corresponding flow parameters are also listed.

To validate the proposed log-linear law, we define the following diagnostic functions:

$$\begin{aligned} \Phi_1 &= \kappa y^+ \frac{\partial U^+}{\partial y^+}, \\ \Phi_2 &= \frac{\kappa y^+ \sqrt{1 + \beta}}{1 + \beta y / \delta_d} \frac{\partial U^+}{\partial y^+}, \end{aligned} \quad (3.1)$$

where Φ_1 and Φ_2 are the diagnostic functions for the conventional log law and the present log-linear law, respectively. This form of diagnostic function has been widely used in previous studies (Monty *et al.* 2011; Pirozzoli 2014). A plateau of $\Phi \approx 1$ indicates that the corresponding law is satisfied.

The diagnostic functions for cases B10B2017–M18B2017 are shown in figure 1, along with the distribution of β with respect to Re_τ . These cases share similar Re_τ but different β values. Only the flow configurations at the middle streamwise stations are considered to avoid inflow and outflow effects. These configurations correspond to the markers in the left column of figure 1. As shown in the middle column of figure 1, the diagnostic function Φ_1

Case	Re_θ	Re_τ	β	Data type	References
B10B2017	1561–2876	400–700	0.9–1.1	LES	Bobke <i>et al.</i> (2017)
B20B2017	1792–3357	400–700	2.0–2.2	LES	Bobke <i>et al.</i> (2017)
M13B2017	1991–3561	450–750	0.9–1.3	LES	Bobke <i>et al.</i> (2017)
M16B2017	2104–3583	450–750	1.8–2.7	LES	Bobke <i>et al.</i> (2017)
M18B2017	2564–3493	450–750	3.1–4.5	LES	Bobke <i>et al.</i> (2017)
B14Y2018	2100–5700	531–803	1.3–1.5	DNS	Yoon <i>et al.</i> (2018)
B14P2022	4808–8359	1000–1800	1.2–1.6	LES	Pozuelo <i>et al.</i> (2022)
B07L2017	1605	364	0.73	DNS	Lee (2017)
B22L2017	2180	346	2.2	DNS	Lee (2017)
B90L2017	2840	318	9.0	DNS	Lee (2017)

Table 1. Summary of the incompressible APG TBL datasets used in the present study. Cases B10B2017, B20B2017, M13B2017, M16B2017, and M18B2017 correspond to cases b1, b2, m13, m16, and m18, respectively, in table 2 of Bobke *et al.* (2017); case B14Y2018 corresponds to the APG TBL case in table 1 of Yoon *et al.* (2018); case B14P2022 corresponds to case b1.4 in table 1 of Pozuelo *et al.* (2022); cases B07L2017, B22L2017, and B90L2017 correspond to cases in table 2 of Lee (2017).

rapidly deviates from 1 in the intermediate regions of the flow. Although the plateau region where $\Phi_1 \approx 1$ appears to extend with the streamwise development, the deviation trend remains unchanged when the wall distance is scaled by the boundary layer thickness, as evidenced by the zoomed views in the middle column. At the same Re_τ , with an increase in β , the deviation of Φ_1 from 1 becomes more pronounced. For example, at $Re_\tau = 517$, the diagnostic function Φ_1 for case B10B2017 with $\beta = 1.0$ exceeds 1.2 at $y^+ = 91$ in the intermediate region, while Φ_1 for case M18B2017 with $\beta = 4.4$ exceeds 1.2 at $y^+ = 79$. By contrast, the diagnostic function Φ_2 shows much better agreement with the plateau of 1 in the intermediate regions and is insensitive to pressure gradient effects.

The same behavior can be observed for cases B14Y2018 and B14P2022, as shown in figure 2. These two cases exhibit similar β but different Re_τ . For the diagnostic function Φ_1 , it can be found that at the same β , with the increase of Re_τ , the deviation of both Φ_1 and Φ_2 from 1 becomes less pronounced. For example, at $\beta = 1.44$, Φ_1 for case B14Y2018 ($Re_\tau = 755$) exceeds 1.2 at $y^+ = 123$, while Φ_1 for case B14P2022 ($Re_\tau = 1267$) exceeds 1.2 at $y^+ = 178$. On the other hand, the diagnostic function Φ_2 exceeds 1.2 at $y^+ = 209$ and $y^+ = 317$ for the same configurations. The Reynolds number effects are to be expected, as the upper boundary of the traditional log region for ZPG TBLs is also proportional to Re_τ (Smits *et al.* 2011). Generally speaking, the plateau of $\Phi_2 \approx 1$ is constantly wider than that of $\Phi_1 \approx 1$ for both cases considered here.

For cases B07L2017–B90L2017, where the Reynolds number is relatively low but β spans a wide range from 0.73 to 9.0, the superiority of the proposed log–linear law is also evident, as shown in figure 3. When the pressure gradient is mild, the difference between Φ_1 and Φ_2 is relatively less distinct, as shown in figure 3(a). However, with an increase in β , the deviation of Φ_1 from 1 becomes pronounced, while Φ_2 maintains a reasonable plateau region of $\Phi_2 \approx 1$, as shown in figures 3(b) and (c).

To quantitatively evaluate the superiority of the proposed log–linear law, we define the effective region of the log law and the log–linear law as the range where the corresponding diagnostic function remains within a tolerance of $\pm 20\%$ of the plateau $\Phi \approx 1$. The span of this region is referred to as the effective length l_e . As shown in figure 4, the effective lengths of the conventional log law are around 0.1δ for most cases, whereas the effective lengths of the log–linear law are consistently larger, with an average value of 0.2δ . Specifically, for the case with the strongest pressure gradients, $\beta = 9.0$ (hexagram marker in figure 4), the

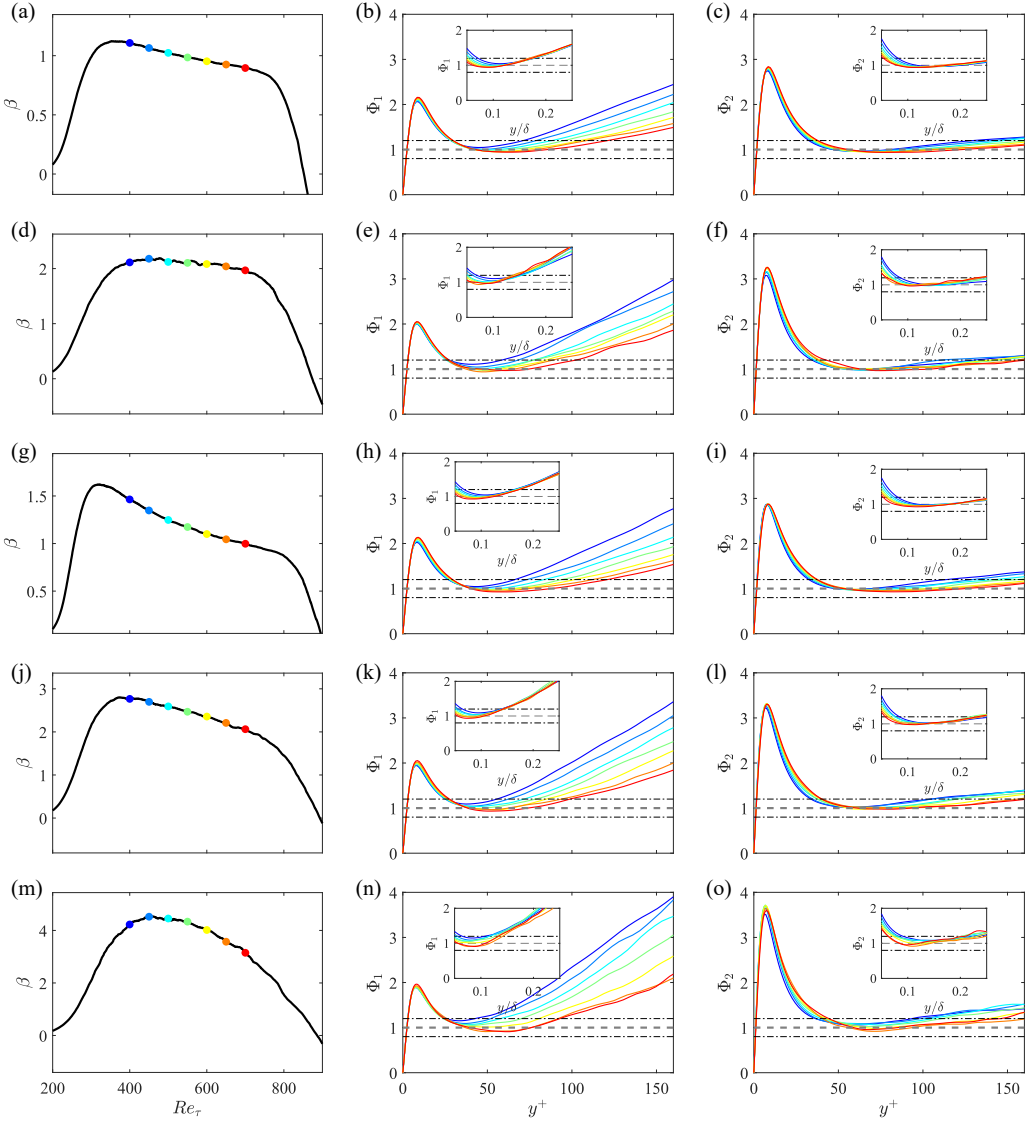


Figure 1. Flow configurations and diagnostic functions for case B10B2017 (a–c), B20B2017 (d–f), M13B2017 (g–i), M16B2017 (j–l), and M18B2017 (m–o). The flow configurations, characterized by the Clauser parameter β and friction Reynolds number Re_τ , are presented by the markers in the left column. The diagnostic functions for the log law (Φ_1) and the log–linear law (Φ_2) are presented in the middle and right columns, respectively. Zoomed views of the diagnostic functions are provided in the insets in the middle and right columns. The horizontal grey dashed line indicates the plateau of $\Phi \approx 1$, with two black dash-dotted lines representing a tolerance of $\pm 20\%$ of the plateau.

effective length of the log law is 0.04δ , while that of the log–linear law is 0.39δ , indicating a nearly 10-fold increase. Therefore, the proposed log–linear law significantly extends the effective region compared to the conventional log law.

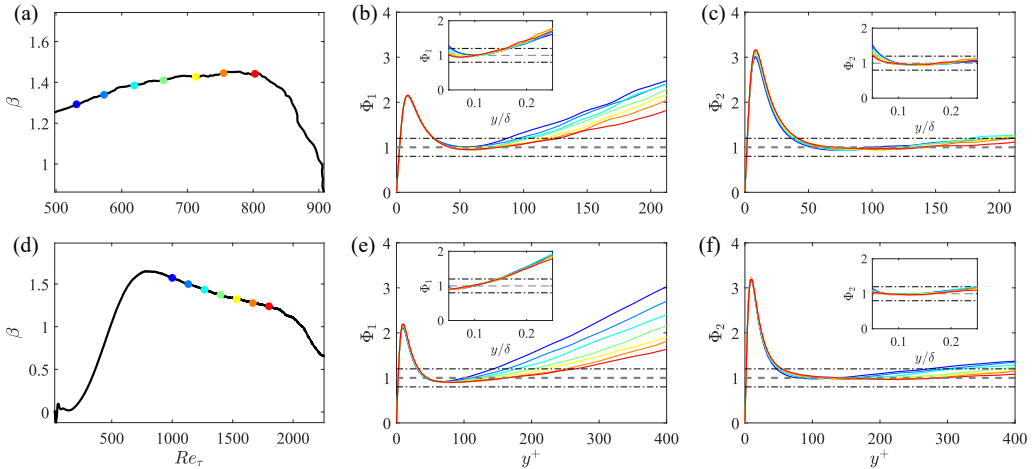


Figure 2. Flow configurations and diagnostic functions for cases B14Y2018 (a–c) and B14P2022 (d–f). The flow configurations, characterized by the Clauser parameter β and friction Reynolds number Re_τ , are presented by the markers in the left column. The diagnostic functions for the log law (Φ_1) and the log–linear law (Φ_2) are presented in the middle and right columns, respectively. Zoomed views of the diagnostic functions are provided in the insets. The horizontal grey dashed line indicates the plateau of $\Phi \approx 1$, with two black dash-dotted lines representing a tolerance of $\pm 20\%$ regarding the plateau.

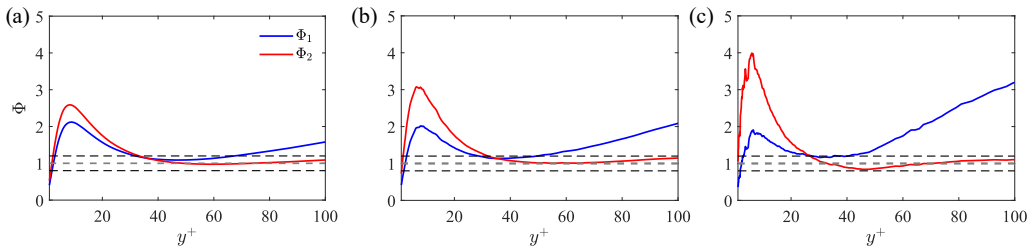


Figure 3. Diagnostic functions for cases B07L2017 (a), B22L2017 (b), and B90L2017 (c). Blue lines and red lines represent the diagnostic functions for the log law and the log–linear law, respectively. The horizontal grey dashed line indicates the plateau of $\Phi \approx 1$, with two black dash-dotted lines representing a tolerance of $\pm 20\%$ regarding the plateau.

4. Conclusions

In this study, we propose a more general velocity law, Eq. (2.9), for the intermediate region of APG TBLs, referred to as the log–linear law. In the limit of zero pressure gradient, the log–linear law reduces to the classical log law. Therefore, the log–linear law can be viewed as a generalization of the conventional log law for APG TBLs. This newly proposed law incorporates a linear term in addition to the logarithmic term. The pressure gradient effects are explicitly accounted for by considering the total shear stress equation and the rescaling of the eddy-viscosity model. It is shown that the log–linear law is superior to the conventional log law, significantly extending the effective range. These results suggest that previous observations of the apparent variation of the Kármán constant κ and the reduction of the effective range of the log law in APG TBLs can be attributed to the inapplicability of the classical log law. Within the framework of the log–linear law, the Kármán constant $\kappa \approx 0.41$ remains unchanged regardless of the pressure gradient. Since the present log–linear law does not involve any additional empirical coefficients, it can be easily implemented in the modeling and prediction of APG TBLs.

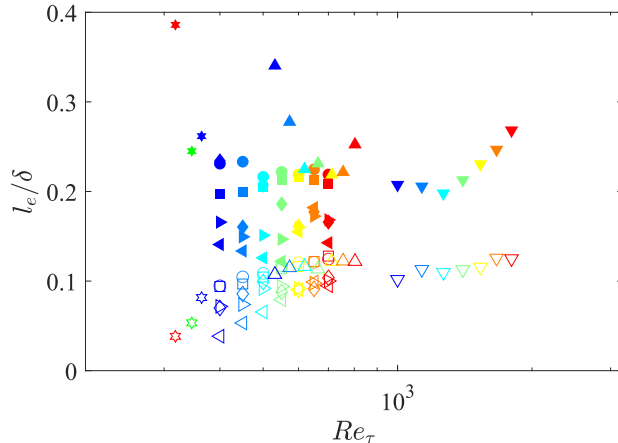


Figure 4. Effective lengths for different cases. Circle, diamond, square, right-triangle, left-triangle, up-triangle, and down-triangle markers correspond to cases B10B2017, B20B2017, M13B2017, M16B2017, M18B2017, B14Y2018, and B14P2022, respectively. The marker colors correspond to the flow configurations in figures 1 and 2. The blue, green, and red hexagrams correspond to cases B07L2017, B22L2017, and B90L2017, respectively. The open and filled markers represent the effective lengths of the log law and the log-linear law, respectively.

REFERENCES

BAGGETT, JEFFREY S 1997 Some modeling requirements for wall models in large eddy simulation. *Annual Research Briefs* **1997**, 265–275.

BOBKЕ, ALEXANDRA, VINUESA, RICARDO, ÖRLÜ, RAMIS & SCHLATTER, PHILIPP 2017 History effects and near equilibrium in adverse-pressure-gradient turbulent boundary layers. *Journal of Fluid Mechanics* **820**, 667–692.

CHAUHAN, KAPIL, NG, HENRY CH & MARUSIC, IVAN 2010 Empirical mode decomposition and hilbert transforms for analysis of oil-film interferograms. *Measurement Science and Technology* **21** (10), 105405.

CLAUSER, FRANCIS H 1954 Turbulent boundary layers in adverse pressure gradients. *Journal of the Aeronautical Sciences* **21** (2), 91–108.

CROOK, A 2002 Skin friction estimation at high reynolds numbers and reynoldsnumber effects for transport aircraft. *Center for Turbulence Research* **164**.

DEVENPORT, WILLIAM J & LOWE, K TODD 2022 Equilibrium and non-equilibrium turbulent boundary layers. *Progress in Aerospace Sciences* **131**, 100807.

HUANG, PG & BRADSHAW, P 1995 Law of the wall for turbulent flows in pressure gradients. *AIAA journal* **33** (4), 624–632.

LARSSON, JOHAN, KAWAI, SOSHI, BODART, JULIEN & BERMEJO-MORENO, IVAN 2016 Large eddy simulation with modeled wall-stress: recent progress and future directions. *Mechanical Engineering Reviews* **3** (1), 15–00418.

LEE, JAE HWA 2017 Large-scale motions in turbulent boundary layers subjected to adverse pressure gradients. *Journal of Fluid Mechanics* **810**, 323–361.

MONTY, JASON P, HARUN, ZAMBRI & MARUSIC, IVAN 2011 A parametric study of adverse pressure gradient turbulent boundary layers. *International Journal of Heat and Fluid Flow* **32** (3), 575–585.

NAGANO, YASUTAKA, TSUJI, TOSHIHIRO & HOURA, TOMOYA 1998 Structure of turbulent boundary layer subjected to adverse pressure gradient. *International Journal of Heat and Fluid Flow* **19** (5), 563–572.

NAGIB, HASSAN M & CHAUHAN, KAPIL A 2008 Variations of von kármán coefficient in canonical flows. *Physics of fluids* **20** (10).

NICKELS, TB 2004 Inner scaling for wall-bounded flows subject to large pressure gradients. *Journal of Fluid Mechanics* **521**, 217–239.

PERRY, AE, MARUŠIĆ, I & LI, JD 1994 Wall turbulence closure based on classical similarity laws and the attached eddy hypothesis. *Physics of Fluids* **6** (2), 1024–1035.

PIROZZOLI, SERGIO 2014 Revisiting the mixing-length hypothesis in the outer part of turbulent wall layers: mean flow and wall friction. *Journal of fluid mechanics* **745**, 378–397.

POPE, STEPHEN B. 2000 *Turbulent Flows*. Cambridge: Cambridge University Press.

POZUELO, RAMÓN, LI, QIANG, SCHLATTER, PHILIPP & VINUESA, RICARDO 2022 An adverse-pressure-gradient

Journal of Fluid Mechanics

turbulent boundary layer with nearly constant $\beta \simeq 1.4$ up to $Re_\theta \simeq 8700$. *Journal of Fluid Mechanics* **939**, A34.

SHU, ZHENGQIN & XU, CHUNXIAO 2025 Mean velocity profiles and total shear stress profiles in adverse-pressure-gradient turbulent boundary layers considering history effect. *arXiv preprint arXiv:2508.07663*

SIMPSON, ROGER L, STRICKLAND, JH & BARR, PW 1977 Features of a separating turbulent boundary layer in the vicinity of separation. *Journal of Fluid Mechanics* **79** (3), 553–594.

SKAARE, PER EGIL & KROGSTAD, PER-ÅGE 1994 A turbulent equilibrium boundary layer near separation. *Journal of Fluid Mechanics* **272**, 319–348.

SMITS, ALEXANDER J, McKEON, BEVERLEY J & MARUSIC, IVAN 2011 High-reynolds number wall turbulence. *Annual Review of Fluid Mechanics* **43** (1), 353–375.

WEI, TIE & KNOPP, TOBIAS 2023 Outer scaling of the mean momentum equation for turbulent boundary layers under adverse pressure gradient. *Journal of Fluid Mechanics* **958**, A9.

WHITE, FRANK M & MAJDALANI, JOSEPH 2006 *Viscous fluid flow*, , vol. 3. McGraw-Hill New York.

WILCOX, DAVID C & OTHERS 1998 *Turbulence modeling for CFD*, , vol. 2. DCW industries La Canada, CA.

YOON, MIN, HWANG, JINYUL & SUNG, HYUNG JIN 2018 Contribution of large-scale motions to the skin friction in a moderate adverse pressure gradient turbulent boundary layer. *Journal of Fluid Mechanics* **848**, 288–311.